Dopamine release dynamics in the tuberoinfundibular dopamine system.

Stefanos Stagkourakis[1*], Johan Dunevall[2], Zahra Taleat[3], Andrew G. Ewing[3] and Christian Broberger[1*]

[1] Department of Neuroscience, Karolinska Institutet, Biomedicum B:4, Solnavägen 9, 171 65 Stockholm, Sweden

[2] Department of Chemistry and Chemical Engineering, Chalmers University of Technology, Kemivägen 10, 41296 Gothenburg, Sweden

[3] Department of Chemistry and Molecular Biology, University of Gothenburg, Kemivägen 10, 41296 Gothenburg, Sweden

*Correspondence: stefanos.stagkourakis@ki.se, christian.broberger@ki.se

ABSTRACT

The relationship between neuronal impulse activity and neurotransmitter release remains elusive. This issue is especially poorly understood in the neuroendocrine system, with its particular demands on periodically voluminous release of neurohormones at the interface of axon terminals and vasculature. A shortage of techniques with sufficient temporal resolution has hindered real-time monitoring of the secretion of the peptides that dominate among the neurohormones. The lactotropic axis provides an important exception, however, as pituitary prolactin secretion is primarily under monoaminergic control, via tuberoinfundibular dopamine (TIDA) neurons projecting to the median eminence (ME). Here, we combined optogenetic stimulation and fast-scan cyclic voltammetry to address dopamine release dynamics in the mouse TIDA system. Imposing different discharge frequencies during brief (3 sec) stimulation of TIDA terminals in the ME revealed that dopamine output is maximal at 10 Hz, which was found to parallel the TIDA neuron action potential frequency distribution. Over more sustained stimulation periods (150 sec), maximal output occurred at 5 Hz. Application of the dopamine transporter blocker, methylphenidate, significantly increased dopamine release in the ME, supporting a functional role of the transporter at the neurons' terminals. Lastly, TIDA neuron stimulation at the cell body yielded perisomatic release of dopamine, which may contribute to an ultra-fast negative feedback mechanism to constrain TIDA electrical activity. Together, these data shed light on how spiking patterns in the neuroendocrine system translate to vesicular release towards the pituitary and identify how dopamine dynamics are controlled in the TIDA system at different cellular compartments.

SIGNIFICANCE STATEMENT A central question in neuroscience is the relationship between neuronal discharge activity and transmitter release. The combination of *e.g.* axonal cable properties and the complex electrical-to-chemical conversion process at the terminal amalgamate to a non-linear process. By combining optogenetic stimulation and voltammetry, we address this issue in dopamine neurons of the neuroendocrine system, which faces particular spatiotemporal demands on exocytotic release. Our data show that release follows an inverted U-shaped distribution, clustering around the neurons' default firing frequency. We further provide support for functional dopamine transport at the neurovascular terminals, shedding light on a long-standing controversy. Finally, we show that dopamine release occurs also at the somatodendritic level, providing a substrate for an ultra-short autoregulatory feedback loop.

INTRODUCTION

The relationship between neuronal impulse traffic and the amount of transmitter released at the axonal terminal has engaged neuroscience since the description of quantal release (Delcastillo & Katz, 1954). A question triggered by these seminal observations on the effects of a single action potential, was how different patterns and frequencies of discharge translate into neurotransmitter exocytosis. The conversion from electrical (action potential) to chemical (Ca^{2+}-dependent vesicle release and subsequent receptor binding) identity of the neuronal signal introduces several non-linearities into the process, which complicate the relationship between discharge pattern and secretion. This issue has been addressed in the well-characterized dopaminergic substantia nigra and ventral tegmental area populations, projecting to the caudate-putamen and nucleus accumbens, respectively, revealing the frequency-dependence of dopamine output (Bass et al, 2010; Zhang et al, 2009). Thus, mesencephalic dopamine terminals exhibit a preferred frequency for optimal neurotransmitter output. Such a mechanism allows neurons to recruit different vesicle and neurotransmitter pools (Doussau et al, 2017; Iverfeldt et al, 1989; Liu et al, 2011), increasing the computational capacity of individual cells. It also provides a safety mechanism, as low activity often will not translate to substantial output (Ngodup et al, 2015).

The neuroendocrine system exhibits several features that distinguishes it from canonical CNS circuits. Thus, instead of a postsynaptic neuron, the targets of the parvocellular systems consist of the endocrine cells of the anterior pituitary gland, which the releasing and inhibiting factors of the neuroendocrine neurones reach by way of the portal capillaries following release at the neurovascular interface (Harris, 1948a; Harris, 1948b). The demands on neurohormone volume that follow from this structural organization likely differ substantially from those required to elicit action within the prototypical synapse. Furthermore, the secretion of signal substances into the blood stream rather than into a confined synaptic cleft suggests that conditions for signal

substance reuptake – if it occurs at all - may be different. These issues have been difficult to explore, however, owing to the lack of temporal high-resolution techniques to quantitatively measure the release of neuropeptides (but see (Glanowska et al, 2012)), which constitute the releasing factors of the neuroendocrine system.

Among the hypothalamo-pituitary systems, the lactotropic axis stands out, however, because of its inhibitory effect on target cells and the monoaminergic nature of its chemical signal. Tuberoinfundibular dopamine (TIDA) neurons located in the dorsomedial arcuate nucleus (dmArc) provide a powerful suppressive influence on pituitary lactotrope cells, which produce the hormone, prolactin (see (Grattan, 2015; Lyons & Broberger, 2014)). Prolactin, in turn, plays an important role in *e.g.* reproduction. A surge in circulating prolactin during late pregnancy and lactation triggers several important physiological functions in the mother including lactation and maternal care (see Grattan, 2015). Dopamine, released in the median eminence (ME) for passage to the hypophyseal portal blood circulation, tonically inhibit the lactotropes through dopamine D2-type receptors (Gudelsky, 1981; Israel et al, 1990; Lledo et al, 1990; Malgaroli et al, 1987; Stefaneanu et al, 2000). Recent studies have revealed distinguishing electrophysiological characteristics of TIDA cells (Lyons et al, 2010), including the capacity for a variable repertoire of firing frequencies in mouse neurons (Romano et al, 2013; Stagkourakis et al, 2018).

Dopamine release can be monitored with high temporal precision and chemical specificity through fast-scan cyclic voltammetry (FSCV; (Baur et al, 1988; Robinson et al, 2003; Rodeberg et al, 2017) . Here, we used optogenetic stimulation (Bass et al, 2010) to impose different discharge protocols upon mouse TIDA neurons and recorded the resultant dopamine release at different cellular compartments. The results provide evidence for frequency optimization, functional reuptake through the dopamine transporter (DAT) at TIDA terminals, and a recently proposed ultra-short autoinhibitory feedback loop (Stagkourakis et al, 2016).

MATERIALS AND METHODS

Animals. All animal experiments had received approval from the local ethical board, *Stockholms Norra Djurförsöksetiska Nämnd*, and were performed in accordance with the European Communities Council Directive of November 24, 1986 (86/609/EEC). Wild-type mice with C57BL/6J and BALB/c background were used, in addition to previously generated C57BL/6J *Slc6a*^{Cre} (DAT-Cre) knock-in (Ekstrand et al, 2007) and floxed-tdTomato mice (The Jackson Laboratory, strain datasheet – 007909). Animals were group-housed, up to five per cage, in a temperature- (23^{o}C) and humidity- (55%) controlled environment, in a 12/12 h light/ dark cycle with *ad libitum* access to food and water. Cages were changed on a weekly basis.

Viral vectors. For channelrhodopsin *in vitro* optogenetic studies animals were microinjected (*vide infra*) in the arcuate nucleus with 250 nL of AAV5-EF1a-DIO-hChR2(H134R)-eYFP-WPRE-hGH (Addgene20298) 8.41×10^{12} genomic copies per mL. Control groups were injected with 250 nL of AAV5-EF1a-DIO-eYFP-WPRE-hGH (Addgene27056) 5.82×10^{12} genomic copies per mL. The ChR2 and control eYFP AAV5's were prepared by the University of Pennsylvania Vector Core.

Stereotactic surgery and viral gene transfer. Adult DAT-Cre male mice of 3 to 6 months age (sexually inexperienced) were stereotactically injected with a virus (*vide supra*) and subsequently individually housed for two weeks post-surgery. Animals were anaesthetized with isoflurane (1–5%) and placed in a stereotaxic frame (David Kopf Instruments). Virus was bilaterally injected into the arcuate nucleus using a pulled glass capillary (World Precision Instruments) by nanolitre pressure injection at a flow rate of 50 nL per min (Micro4 controller, World Precision Instruments; Nanojector II, Drummond Scientific). Stereotactic injection coordinates (Bregma: -1.8 mm, midline ±0.1 mm, dorsal surface -5.5 mm) to target the dmArc were obtained from the Paxinos and Franklin atlas (Franklin & Paxinos, 2008).

Brain slice electrophysiology. Acute slices of the mediobasal hypothalamus were prepared from adult DAT-tdTomato mice. Slices were cut on a vibratome (Leica VT1000S) to 250 µm thickness and continuously perfused with oxygenated aCSF containing (in millimolar): NaCl (127), KCl (2.0), NaH_2PO_4 (1.2), $NaHCO_3$ (26), $MgCl_2$ (1.3), $CaCl_2$ (2.4), and D-glucose (10), at 32±1°C during recording. Each slice was exposed only to a single bath application of pharmacological compounds and was used for a single experiment. Whole-cell current- and voltage-clamp recordings were performed with micropipettes filled with intracellular solution containing (in millimolar), K-gluconate (140), KCl (10), HEPES (10), EGTA (10), and Na_2ATP (2) (pH 7.3 with KOH). Recordings were performed using a Multiclamp 700B amplifier, a DigiData 1440 digitizer, and pClamp 10.2 software (Molecular Devices). Slow and fast capacitative components were semi-automatically compensated. Access resistance was monitored throughout the experiments, and neurons in which the series resistance exceeded 15 MΩ or changed ≥20% were excluded from further analysis. Liquid junction potential was 16.4 mV and not compensated. The recorded current was sampled at 20 kHz.

For *in vitro* optogenetics during slice whole-cell recordings, photostimulation was generated through a 3.4 watt 447 nm LED mounted on the microscope oculars and delivered through the objective lens. Photostimulation was controlled via the analogue outputs of a DigiData 1440A, enabling control over the duration and intensity. The photostimulation diameter through the objective lens was ~350 µm with illumination intensity typically scaled to 3 mW/mm^2. Methylphenidate hydrochloride (M2892 – SIGMA), dissolved in aCSF, was bath applied via gravitational flow. Matlab and OriginPro8 were used for electrophysiological data analysis.

Immunofluorescence. Mice were anaesthetised with sodium pentobarbital (200 mg/kg, i.p., Sanofi-Aventis), then transcardially perfused with 10 mL Ca^{2+}-free Tyrode's solution (37°C) containing 0.2% heparin, followed by 10 mL fixative (4% paraformaldehyde and 0.4% picric acid in 0.16 M phosphate buffer (PBS), 37°C), then 50 mL ice cold fixative. Whole brains were dissected, immersed in ice-cold fixative for 90 min then stored in 0.1M PBS (pH 7.4) containing 20% sucrose, 0.02% bacitracin and 0.01% sodium azide for

three days, before freezing with CO_2. Coronal sections were cut at a thickness of 14 µm using a cryostat (Microm) and thaw-mounted onto gelatin-coated glass slides. For indirect immunofluorescence staining (performed at room temperature unless otherwise specified), air-dried sections were washed in 0.01 M PBS for 30 min before incubation with the primary antibody diluted in PBS containing 0.3% Triton X-100 and 1% BSA for 16 hours at 4°C. The slides were then washed for 30 min in PBS followed by 2h incubation with Alexa-488-conjugated donkey anti-rabbit secondary antisera (1:500; Invitrogen). Slides were incubated with the nuclear marker 4',6-diamidino-2-phenylindole (DAPI; Invitrogen) diluted 1: 10,000 in PBS for five min before a final wash for 30 min in PBS and mounted with glycerol containing (2.5% DABCO; Sigma).

In situ **hybridization.** DAT-Cre-floxed-tdTomato mice were anaesthetized with pentobarbital, sacrificed by decapitation, and the brains were rapidly removed and frozen on dry ice. 10 µm-thick coronal sections were cut using a cryostat and thaw-mounted onto SuperFrost glass slides. Sections were fixed in 4% PFA for 15 min at 4°C and then dehydrated through incubation in 50% EtOH (1 X 5 min), 70% EtOH (1 X 5 min) and lastly 100% EtOH (2 X 5 min). Slides were air dried for 10 min and a hydrophobic barrier was created around each section using the ImmEdge™ pen (Vector laboratories). *In situ* hybridization was performed using a modification of the RNAScope® (Advanced Cell Diagnostics) protocol. Pretreat 4 (ACDBio, RNAscope® Fluorescent Multiplex Reagent Kit, 320850) was added to entirely cover the sections for 30 min at room temperature. After PBS washing, sections were incubated with Mm-Slc6a3-C2 (315441-C2) and tdTomato (317041) RNAscope® probes for 2h at 40°C using the HybEZ™ Humidifying System. The following incubation steps were then performed: Amp 1-FL for 30 min at 40°C, Amp 2-FL for 15 min at 40°C, Amp 3-FL for 30 min at 40°C and Amp 4-FL-AltB for 15 min at 40°C (320850). Wash buffer (320850) was used to rinse the slides after each step. Sections were incubated with DAPI solution (320850) for 30 sec at room temperature and ProLong Gold Antifade Mountant (Thermo Fisher Scientific) was added before placing the coverslips. Quantification of mRNA coexistence within cells was performed on confocal Z-stack arcuate nucleus images acquired at 40X magnification.

Confocal microscopy. Brain slices were imaged by epifluorescence microscopy (Zeiss Imager M1) or confocal microscopy (Zeiss, LSM 800) for subsequent analysis. Brain areas were determined according to their anatomy using Paxinos and Franklin brain atlas (Franklin & Paxinos, 2008).

Carbon Fiber Microelectrodes. Carbon fiber electrodes were fabricated by aspirating 7 µm diameter carbon fibers (Cytec engineered materials, Tempe, AZ) into borosilicate glass capillaries (1.2 mm O.D., 0.69 mm I.D., Sutter Instrument Co., Novato, CA). The capillaries were subsequently pulled with a commercial micropipette puller (Sutter Instrument, P-97) and sealed with epoxy (EpoTek 301, Epoxy Technology, Billerica). The electrode tips were polished at a 45° angle on a diamond dust-embedded micropipette-bevelling wheel (Model BV-10, Sutter Instrument Co.). Electrodes were tested in solutions of known concentrations of dopamine. Only electrodes showing reaction kinetics typical of dopamine (as examined in current *vs* time plots, and current *vs* voltage plots) were used.

Fast-Scan Cyclic Voltammetry. A Dagan Chem-Clamp potentiostat (Dagan Corporation, Minneapolis, MN) and two data acquisition boards (PCI-6221, National Instruments) run by the TH 1.0 CV program (ESA) were used to collect all electrochemical data. Cyclic voltammograms were obtained by applying a triangular waveform potential (−0.4 to +1.3 V *vs* Ag/AgCl) repeated every 100 ms at a scan rate of 200 V/s (low pass Bessel filter at 3 kHz). Each cyclic voltammogram was a background-subtracted average of ten successive cyclic voltammograms taken at the maximum oxidation peak current. All electrodes were allowed to cycle for at least 15 min prior to recording to stabilize the background current. The recorded current response was converted to dopamine concentration via *in vitro* electrode calibration in a standard dopamine solution after each experiment. Acquired data were analysed and plotted using Matlab routines and statistical analysis was performed using Prism 6.0 (GraphPad Software). Lastly, bath application of the DAT blocker methylphenidate in isolation (*i.e.* in the absence of a brain slice), did not generate oxidative current during FSCV recordings (n=3).

Experimental design and statistical analysis. Acquisition of fast-scan cyclic voltammetry data was performed for each dataset on brain slices collected from a minimum of three individual animals on consequent experimental days. A minimum of five recordings represent each FSCV group. Acquisition of electrophysiology and immunohistochemistry data followed the same experimental design. All *t*-tests and one-way ANOVAs were performed using Graph Pad Prism software (Graphpad Software). The appropriate post hoc test was used for each one-way ANOVA. Normality was determined by D'Agostino–Pearson normality test. Statistical significance was set at $P < 0.05$.

RESULTS

Absence of detectable spontaneous dopamine release in coronal hypothalamic slices

TIDA neurons (Fig. 1*A*) were targeted for recording using DAT-tdTomato mice (Fig. 1*B-D*). To evaluate the DAT-Cre mouse line as an appropriate model for identifying TIDA cells, we performed double-label *in situ* hybridization for DAT and tdTomato in hypothalamic brain sections from DAT-tdTomato mice. A near 100% colocalization was found between the two mRNA species, validating the expression of Cre in TIDA neurons (*i.e.* dopaminergic neurons in the dmArc; Fig. 1*F*).

Whole-cell patch clamp recordings confirmed that mouse TIDA neurons exhibit a diverse range of firing rates *in vitro* in agreement with earlier reports (Romano et al, 2013; Stagkourakis et al, 2018; Zhang & van den Pol, 2015); Fig. 1*G*). The majority of TIDA cells were found to have a tonic firing pattern with phasic alterations in firing frequency, echoed in phasic fluctuations in membrane voltage (Fig. 1*G*, middle). *Circa* one-fourth of the cells exhibited oscillatory, rhythmic firing interspersed with brief (~500 ms) periods of quiescence (Fig. 1*G*, left). A small fraction of the TIDA neurons in the slice preparation were consistently hyperpolarized and quiescent (Fig. 1*G*, right).

As TIDA neurons are spontaneously active *in vitro*, we first asked if baseline dopamine release can be detected at the site of the terminals in the slice preparation. Carbon fiber electrodes were thus placed in the ME, and an adapted FSCV protocol from (Kosillo et al, 2016) was applied (Fig. 1*H*). In this configuration, no dopamine signal could be observed above the detection threshold (~10 nM; *N*=20 recordings from *N*=10 slices from *N*=5 mice; Fig. 1*I-K*). One possible reason for this failure to detect dopamine may be that the axons connecting the TIDA cell somata in the dmArc and the terminals in the ME have been severed when producing the coronal slice preparation (van den Pol & Cassidy, 1982), interrupting impulse traffic. We therefore next sought to identify evoked dopamine release properties via optogenetic stimulation of the TIDA terminals. This

strategy offers the benefit that the dynamics of the transmitter release at the level of the terminals, on the one hand, and at the somatodendritic level on the other, can be studied separately.

Stable optically evoked dopamine release in the median eminence

To enable dopamine release from the terminals, DAT-Cre animals were bilaterally injected into the dmArc with AAV-DIO-ChR2. One month later, FSCV recordings were performed *in vitro* to test for optically evoked dopamine release (Fig. *2*A). Using a stimulation protocol of 5 s in duration and 10 Hz frequency stimulation with 5 ms pulse width, robust and stable dopamine release was recorded from the ME (Fig. 2*B*). To test for the possibility of dopamine depletion at the terminals with repeated stimulation, we performed recurrent photostimulation at different time intervals (1 or 5 min). Photostimulation with 5 min intervals resulted in stable evoked release at near 100 % of the initial levels, throughout a 30 min period (Fig. 2*C*; $N = 7$, $F_{(3.161, 18.96)} = 0.2747$, df = 6, $p = 0.8522$, RM one-way ANOVA; see also Table 1). Photostimulation with 1 min intervals resulted in attenuation of the dopamine signal to near 50 % of the basal levels over ten minutes (Fig. 2D; $N = 5$, $F_{(3.036, 12.14)} = 2.188$, df = 14, $p = 0.1413$, RM one-way ANOVA; see also Table 1). Once the longer (5 min) photostimulation interval was reinstated, however, the dopamine signal recovered to initial levels (Fig. 2D).

Frequency preference for maximal dopamine release at the level of the terminals matches the endogenous average firing frequency of TIDA neurons

The majority of action potentials in the UP states of spontaneously active TIDA neurons (Fig. 3A) are discharged within a *ca*. 10 Hz frequency (Fig. 3*B*; $N = 33$, $F_{(14, 338)} = 17.08$, df = 14, $p < 0.0001$, one-way ANOVA with Tukey's test; see also Table 1), and the instantaneous frequency follows a normal-like distribution with a peak at 10.02 Hz (Fig. 3*A, C*). Following the characterization of the ChR2-mediated current with a fast and a slow component (Fig. 3*D*; $N = 6$, t = 4.357, df = 5, $p = 0.0073$, two-tailed paired *t* test; see also Table 1) in somatic recordings, we investigated the spike fidelity of the TIDA cells at

different photostimulation frequencies. Optogenetic stimulation of ChR2-transduced DAT-Cre neurons at frequencies of ≤10 Hz yielded a 100% spike fidelity (Fig. 3*E* top trace, 3*F*; see also Table 1), while higher photostimulation frequencies (30-50 Hz) led to a depolarization block phase with substantial spike failure (Fig. 3*E* bottom trace, 3*F*; see also Table 1). The latter phenomenon has previously been described in rat TIDA cells in response to pharmacological manipulations (Stagkourakis et al, 2016).

Based on the observation that spontaneous TIDA discharge is strongly biased to the 10Hz frequency band, we next addressed if specific stimulation frequencies of the TIDA terminals are associated with more or less efficient transmitter release. To investigate this issue, a brief (3 s) photostimulation protocol was applied at frequencies ranging from 2 to 50 Hz. Maximal dopamine release was recorded at 10 Hz, with both higher and lower frequencies eliciting less dopamine signal (Fig. 3*G, H*). Importantly, the 10Hz frequency yielded optimal dopamine release regardless of pulse duration (Fig. 3*H*; see also Table 1). Together, these data suggest that the membrane properties of TIDA neurons, at the somatodendritic and axon terminal levels, are optimized to both discharge and release neurotransmitter content at 10 Hz.

As dopamine release dynamics may vary between short and long bouts of activity, we repeated the analysis of the frequency- and pulse duration-dependence of dopamine release using a longer-duration (150 s) photostimulation protocol. The maximal dopamine release signal was also here biased towards the slower frequencies, with the greatest value recorded at 2-5 Hz (Fig. 4*A*-*E*; see also Table 1).

Functional dopamine transporter in the median eminence

The expression of DAT in TIDA neurons is well documented (Meister & Elde, 1993; Revay et al, 1996; Demaria et al, 2000a; Stagkourakis et al, 2018), yet, the functional role of the transporter within the lactotropic axis remains controversial (Annunziato et al, 1980;

Bosse et al, 1997; Demarest & Moore, 1979; Demaria et al, 2000a; Meister & Elde, 1993; Revay et al, 1996; Stagkourakis et al, 2018). To assess if reuptake is involved at determining dopamine levels at the entry to the portal vasculature, we performed optogenetic stimulation of TIDA terminals in the ME, in the absence and presence of the clinically prescribed DAT blocker, methylphenidate (Taylor & Ho, 1978; Volkow et al, 1999a; Volkow et al, 1999b). Following application of methylphenidate (Fig. 5A) the photostimulation-induced dopamine signal was augmented, quantified as prolonged decay (Fig. 5*B*; $N = 6$, t = 4.439, df = 5, $p = 0.0068$, two-tailed paired *t* test) and half-width (Fig. 5*D*; $N = 6$, t = 5.228, df = 5, $p = 0.0034$, two-tailed paired *t* test), whereas maximal [dopamine] release and rise time were not affected (Fig. 5*C, D*; see also Table 1). These data suggest the presence of functional dopamine transport active in the ME.

Capacity for dopamine release at the somatodendritic compartment of TIDA neurons

Recent work has suggested that local release of dopamine around the cell body and dendrites of TIDA neurons may serve as a critical component of an ultra-short feedback loop that tunes the electrical activity of these neurons to their recent transmitter secretion history (Belousov & vandenPol, 1997; Durham et al, 1998; Liang et al, 2014; Liang & Pan, 2012; Stagkourakis et al, 2016). Yet to date, no direct evidence exists that dopamine can indeed be released in the somatodendritic compartment in the dmArc. To investigate this possibility, TIDA cells were transduced with ChR2-eYFP. Inspection of cryostat sections of the dmArc of such animals revealed that the ChR2 construct was distributed on both cell bodies and dendrites of DAT-tdTomato-positive neurons (Fig. 6*A*). We next performed FSCV recordings in the dmArc with the carbon fibre electrode placed in the area occupied by TIDA cell somata (Fig. 6*B*). As in the ME (*vide supra*), no spontaneous release could be recorded. When photostimulation was performed using the 5sec duration/10Hz/5ms pulse protocol found to evoke optimal release in the ME (Fig. 3*H*), however, a distinct dopamine signal could be recorded (Fig. 6*C, D*). This signal was typically 10-20-fold below that recorded in the ME (compare figures Fig. 6*D* and Fig. 3*H*). A photostimulation artifact is evident at ca. 0 V and +1.3V in the voltammogram,

352 similar to what has been described previously (Bass et al, 2013). These results provide
353 strong evidence for a capacity for dopamine release at the cell body level of TIDA
354 neurons.

355

356

DISCUSSION

The ability of a neuron to translate electrical activity to chemical signal is a core feature of the nervous system. Studies of dopamine transmission in the basal ganglia *e.g.* have identified several principles of stimulus-secretion coupling (Bass et al, 2010; Oleson et al, 2009; Sulzer et al, 2016; Zhang et al, 2009). Yet, the specific volume and coding demands of transmitter release facing different brain systems are likely to vary depending on their role in behaviour and physiology. Here, we addressed this issue in the neuroendocrine parvocellular system, where transmitter release from TIDA neurons can be monitored by FSCV and spiking patterns manipulated by optogenetic control.

We show that while mouse TIDA neurons are able to spike across a spectrum of frequencies, in agreement with previous studies (Romano et al., 2013, Zhang and van den Pol, 2015; Stagkourakis et al., 2018), action potentials are primarily discharged within a 10Hz frequency band. When depolarized with greater stimulation than required to reach this frequency, TIDA neurons are successively more prone to depolarization block and spike failure (present data and Stagkourakis et al., 2016). Importantly, maximal dopamine release was also accomplished with a 10Hz stimulation frequency (concomitant with full spike fidelity). Thus, the system appears to be operating at full capacity at its default spike rate (although it should be borne in mind that *in vivo* discharge frequencies – currently not known for the TIDA system - may be different). These results were recorded with 3 s stimulation bouts, in the range of the typical TIDA oscillation UP state in subthreshold oscillating cells (Stagkourakis et al., 2018). For extended periods (150 s) of stimulation, the optimal frequency was shifted towards slower frequencies. In the context of these findings, it can be noted that sustained (tonic) firing is triggered in TIDA neurons by modulators associated with inhibition of prolactin release upon central administration (Lyons et al., 2010; 2012; 2017; Briffaud et al., 2015). The firing frequency during this transmitter/hormone-induced persistent discharge can be lower than in the oscillatory state (Lyons et al., 2010), which may then

offer an adaptation to the extended firing/lower frequency principle for optimal transmitter release suggested by the present data.

The dopamine concentration elicited by optogenetic stimulation ranged within ca. 0.5-1.5 µM, *ca*. ten times above that recorded in the intact striatum following a single impulse, or one hundred times higher than baseline striatal levels (see Sulzer et al., 2016). The comparison between brain regions and *in vivo* and *in vitro* conditions is fraught with complications, but it may be speculated that greater dopamine concentrations are required to activate targets in the tuberoinfundibular than in the nigrostriatal pathway. But an additional possibility could be that excess of dopamine is necessary to compensate for the relatively less precise delivery of dopamine across the neurovascular interface and capillary distribution system compared to the point-to-point synaptic transmission in the striatum. It can also be noted that the levels we recorded are several magnitudes above those required for activation of D2R autoreceptors (Gonon & Buda, 1985), which may be present on the somatodendritic compartments or TIDA terminals (Berry & Gudelsky, 1991; Huang et al, 2013; Stagkourakis et al, 2016).

Previous *in vitro* (Romano et al, 2013) and *in vivo* (Romano et al, 2017) amperometry investigations have indicated that increased firing (induced by prolactin administration) in the TIDA ensemble correlates to higher amperometric signal at the terminal level, and that a range of release even frequencies can be detected in the ME in the intact animal. Yet, a comprehensive understanding of the coupling between TIDA neuron activity and dopamine release at the terminals has been lacking. The superior ability of FSCV over amperometry to identify transmitters with chemical selectivity (Bucher & Wightman, 2015), combined with the msec precision control spiking through optogenetics, has allowed us in the current study to correlate specific firing patterns to dopamine release volumes in the TIDA system, without contamination of other transmitters and metabolites.

The role of DAT in TIDA neurons has been a subject of controversy. Pharmacological studies of dopamine accumulation initially suggested that dopamine reuptake had a minor effect on ME levels, leading to conclusions that a transporter system was not reconcilable with vascular release (Annunziato et al, 1980; Demarest & Moore, 1979). This conclusion has however been challenged by subsequent studies using other DAT antagonists (Demaria et al, 2000b) and genetic deletion (Bosse et al, 1997). Here, we show that optogenetically elicited dopamine release at the ME is powerfully amplified in the presence of methylphenidate, a clinically used antagonist of DAT. It is important to remember in this context that neuroendocrine neurons do not make immediate contact with portal capillaries, but rather abut a perivascular space (Ajika & Hokfelt, 1973) where release is postulated to occur. This organization suggests that secreted dopamine may linger for a period in the proximity of the terminal prior to ending up in the blood stream, allowing for a window of opportunity for transmitter reuptake.

Recently, we have proposed the existence of an ultra-short D2R-mediated feedback loop (Stagkourakis et al., 2016). This model is primarily based on pharmacological and electrophysiological findings, but a key component of this scheme is the existence of release of ambient dopamine at the somatodendritic compartment, for which evidence has been lacking. The present study shows that release of dopamine can be triggered at the cell body level through optogenetic stimulation. Notably, the levels thus elicited were *ca.* a magnitude lower than what was recorded in the ME with similar stimulation. Our model proposes that local dmArc release mirrors fluctuations at the ME, but need not do so at similar absolute concentrations. Thus, the current findings support the existence of an autoinhibitory feedback loop. The exact release site for this evoked dopamine remains to be determined. Ultrastructural studies have demonstrated that TIDA neurons extend recurrent collaterals that project towards, but do not make direct contact with, TIDA cell bodies (Piotte et al, 1985), which could be providing extrasynaptic dopamine. There are, however, also dense dendrodendritic and somatodendritic contacts within the TIDA population (Piotte et al, 1985). In the midbrain, such contacts have been implicated in local release from the soma and/or dendrites (Cheramy et al,

1981; Hefti & Lichtensteiger, 1978; Rice & Patel, 2015). The current findings suggest that this possibility merits further investigation in the TIDA system.

In summary, the present data show how dopamine dynamics in the TIDA system correlate to spike rates, and identify regulatory mechanisms involved in this process at both the terminal and somatodendritic level. These findings offer insight into the relationship between electrical activity and signal substance release in the neuroendocrine system, and provide a platform for further investigations of stimulus-secretion coupling in the hypothalamo-pituitary axis.

Competing interests: The authors declare no competing interests.

Acknowledgments: The authors thank Paul Williams for providing insightful suggestions on the manuscript, Elin Dahlberg and Sandra Azami for expert technical support, and Dr. Nils-Göran Larsson for generously sharing DAT-Cre mice.

Funding: This study was supported by a European Research Council (ERC) Starting Grant (ENDOSWITCH; 261286), the Swedish Research Council (2014-3906), the Strategic Research Program in Diabetes at Karolinska Institutet, *Hjärnfonden* (the Swedish Brain Foundation), *Novo Nordisk Fonden* and internal funds from Karolinska Institutet to C.B., and grants from the ERC (Advanced Grant), the Swedish Research Council and the Knut and Alice Wallenberg Foundation to A.G.E.

Author contributions: S.S. and C.B. designed experiments. S.S. performed the experiments. S.T., J.D., R.T., E.C.B., and A.G.E. set up and assisted with the implementation of FSCV. S.S. and C.B. wrote the manuscript. All authors reviewed and commented on the manuscript.

REFERENCES

Ajika K, Hokfelt T (1973) Ultrastructural identification of catecholamine neurones in the hypothalamic periventricular-arcuate nucleus-median eminence complex with special reference to quantitative aspects. *Brain research* **57:** 97-117

Annunziato L, Leblanc P, Kordon C, Weiner RI (1980) Differences in the Kinetics of Dopamine Uptake in Synaptosome Preparations of the Median-Eminence Relative to Other Dopaminergically Inervated Brain-Regions. *Neuroendocrinology* **31:** 316-320

Bass CE, Grinevich VP, Kulikova AD, Bonin KD, Budygin EA (2013) Terminal effects of optogenetic stimulation on dopamine dynamics in rat striatum. *Journal of neuroscience methods* **214:** 149-155

Bass CE, Grinevich VP, Vance ZB, Sullivan RP, Bonin KD, Budygin EA (2010) Optogenetic control of striatal dopamine release in rats. *Journal of neurochemistry* **114:** 1344-1352

Baur JE, Kristensen EW, May LJ, Wiedemann DJ, Wightman RM (1988) Fast-scan voltammetry of biogenic amines. *Analytical chemistry* **60:** 1268-1272

Belousov AB, vandenPol AN (1997) Dopamine inhibition: Enhancement of GABA activity and potassium channel activation in hypothalamic and arcuate nucleus neurons. *Journal of neurophysiology* **78:** 674-688

Berry SA, Gudelsky GA (1991) Effect of D2 Dopamine Agonists on Tuberoinfundibular Dopamine Neurons. *Neuropharmacology* **30:** 961-965

Bosse R, Fumagalli F, Jaber M, Giros B, Gainetdinov RR, Wetsel WC, Missale C, Caron MG (1997) Anterior pituitary hypoplasia and dwarfism in mice lacking the dopamine transporter. *Neuron* **19:** 127-138

Bucher ES, Wightman RM (2015) Electrochemical Analysis of Neurotransmitters. *Annu Rev Anal Chem* **8:** 239-261

Cheramy A, Leviel V, Glowinski J (1981) Dendritic release of dopamine in the substantia nigra. *Nature* **289:** 537-542

Delcastillo J, Katz B (1954) Quantal Components of the End-Plate Potential. *J Physiol-London* **124:** 560-573

Demarest KT, Moore KE (1979) Lack of a High-Affinity Transport-System for Dopamine in the Median-Eminence and Posterior Pituitary. *Brain research* **171:** 545-551

Demaria JE, Nagy GM, Lerant AA, Fekete MI, Levenson CW, Freeman ME (2000a) Dopamine transporters participate in the physiological regulation of prolactin. *Endocrinology* **141:** 366-374

Demaria JE, Nagy GM, Lerant AA, Fekete MIE, Levenson CW, Freeman ME (2000b) Dopamine transporters participate in the physiological regulation of prolactin. *Endocrinology* **141:** 366-374

Doussau F, Schmidt H, Dorgans K, Valera AM, Poulain B, Isope P (2017) Frequency-dependent mobilization of heterogeneous pools of synaptic vesicles shapes presynaptic plasticity. *eLife* **6**

Durham RA, Johnson JD, Eaton MJ, Moore KE, Lookingland KJ (1998) Opposing roles for dopamine D-1 and D-2 receptors in the regulation of hypothalamic tuberoinfundibular dopamine neurons. *European journal of pharmacology* **355:** 141-147

Ekstrand MI, Terzioglu M, Galter D, Zhu S, Hofstetter C, Lindqvist E, Thams S, Bergstrand A, Hansson FS, Trifunovic A, Hoffer B, Cullheim S, Mohammed AH, Olson L, Larsson NG (2007) Progressive parkinsonism in mice with respiratory-chain-deficient dopamine neurons. *Proceedings of the National Academy of Sciences of the United States of America* **104:** 1325-1330

Franklin KBJ, Paxinos G (2008) *THE MOUSE BRAIN IN STEREOTACTIC COORDINATES*, Vol. Third edition.

Glanowska KM, Venton BJ, Moenter SM (2012) Fast Scan Cyclic Voltammetry as a Novel Method for Detection of Real-Time Gonadotropin-Releasing Hormone Release in Mouse Brain Slices. *Journal of Neuroscience* **32:** 14664-14669

Gonon FG, Buda MJ (1985) Regulation of Dopamine Release by Impulse Flow and by Autoreceptors as Studied by Invivo Voltammetry in the Rat Striatum. *Neuroscience* **14:** 765-774

Grattan DR (2015) 60 Years of Neuroendocrinology the Hypothalamo-Prolactin Axis. *Journal of Endocrinology* **226:** T101-T122

Gudelsky GA (1981) Tuberoinfundibular Dopamine Neurons and the Regulation of Prolactin Secretion. *Psychoneuroendocrinology* **6:** 3-16

Harris GW (1948a) Electrical Stimulation of the Hypothalamus and the Mechanism of Neural Control of the Adenohypophysis. *J Physiol-London* **107:** 418-+

Harris GW (1948b) Neural Control of the Pituitary Gland. *Physiological reviews* **28:** 139-179

555 Hefti F, Lichtensteiger W (1978) Dendritic Dopamine - Studies on Release of Endogenous
556 Dopamine from Subcellular Particles Derived from Dendrites of Rat Nigro-Striatal Neurons.
557 *Neuroscience letters* **10:** 65-70

558
559 Huang RQ, Griffin SA, Taylor M, Vangveravong S, Mach RH, Dillon GH, Luedtke RR (2013) The
560 Effect of SV 293, a D2 Dopamine Receptor-Selective Antagonist, on D2 Receptor-Mediated GIRK
561 Channel Activation and Adenylyl Cyclase Inhibition. *Pharmacology* **92:** 84-89

562
563 Israel JM, Kukstas LA, Vincent JD (1990) Plateau Potentials Recorded from Lactating Rat Enriched
564 Lactotroph Cells Are Triggered by Thyrotropin-Releasing-Hormone and Shortened by Dopamine.
565 *Neuroendocrinology* **51:** 113-122

566
567 Iverfeldt K, Serfozo P, Arnesto LD, Bartfai T (1989) Differential Release of Coexisting
568 Neurotransmitters - Frequency-Dependence of the Efflux of Substance-P, Thyrotropin Releasing
569 Hormone and [H-3] Serotonin from Tissue-Slices of Rat Ventral Spinal-Cord. *Acta physiologica*
570 *Scandinavica* **137:** 63-71

571
572 Kosillo P, Zhang YF, Threlfell S, Cragg SJ (2016) Cortical Control of Striatal Dopamine Transmission
573 via Striatal Cholinergic Interneurons. *Cerebral cortex*

574
575 Liang SL, Hsu SC, Pan JT (2014) Involvement of dopamine D-2 receptor in the diurnal changes of
576 tuberoinfundibular dopaminergic neuron activity and prolactin secretion in female rats. *Journal*
577 *of biomedical science* **21**

578
579 Liang SL, Pan JT (2012) An endogenous dopaminergic tone acting on dopamine D-3 receptors
580 may be involved in diurnal changes of tuberoinfundibular dopaminergic neuron activity and
581 prolactin secretion in estrogen-primed ovariectomized rats. *Brain research bulletin* **87:** 334-339

582
583 Liu XH, Porteous R, de Tassigny XD, Colledge WH, Millar R, Petersen SL, Herbison AE (2011)
584 Frequency-Dependent Recruitment of Fast Amino Acid and Slow Neuropeptide
585 Neurotransmitter Release Controls Gonadotropin-Releasing Hormone Neuron Excitability.
586 *Journal of Neuroscience* **31:** 2421-2430

587
588 Lledo PM, Legendre P, Israel JM, Vincent JD (1990) Dopamine Inhibits 2 Characterized Voltage-
589 Dependent Calcium Currents in Identified Rat Lactotroph Cells. *Endocrinology* **127:** 990-1001

590
591 Lyons DJ, Broberger C (2014) TIDAL WAVES: Network mechanisms in the neuroendocrine control
592 of prolactin release. *Frontiers in neuroendocrinology* **35:** 420-438

593
594 Lyons DJ, Horjales-Araujo E, Broberger C (2010) Synchronized network oscillations in rat
595 tuberoinfundibular dopamine neurons: switch to tonic discharge by thyrotropin-releasing
596 hormone. *Neuron* **65:** 217-229

597

Malgaroli A, Vallar L, Elahi FR, Pozzan T, Spada A, Meldolesi J (1987) Dopamine Inhibits Cytosolic-Ca-2+ Increases in Rat Lactotroph Cells - Evidence of a Dual Mechanism of Action. *Journal of Biological Chemistry* **262:** 13920-13927

Meister B, Elde R (1993) Dopamine transporter mRNA in neurons of the rat hypothalamus. *Neuroendocrinology* **58:** 388-395

Ngodup T, Goetz JA, McGuire BC, Sun W, Lauer AM, Xu-Friedman MA (2015) Activity-dependent, homeostatic regulation of neurotransmitter release from auditory nerve fibers. *Proceedings of the National Academy of Sciences of the United States of America* **112:** 6479-6484

Oleson EB, Salek J, Bonin KD, Jones SR, Budygin EA (2009) Real-time voltammetric detection of cocaine-induced dopamine changes in the striatum of freely moving mice. *Neuroscience letters* **467:** 144-146

Piotte M, Beaudet A, Joh TH, Brawer JR (1985) The fine structural organization of tyrosine hydroxylase immunoreactive neurons in rat arcuate nucleus. *The Journal of comparative neurology* **239:** 44-53

Revay R, Vaughan R, Grant S, Kuhar MJ (1996) Dopamine transporter immunohistochemistry in median eminence, amygdala, and other areas of the rat brain. *Synapse* **22:** 93-99

Rice ME, Patel JC (2015) Somatodendritic dopamine release: recent mechanistic insights. *Philosophical transactions of the Royal Society of London Series B, Biological sciences* **370**

Robinson DL, Venton BJ, Heien ML, Wightman RM (2003) Detecting subsecond dopamine release with fast-scan cyclic voltammetry in vivo. *Clinical chemistry* **49:** 1763-1773

Rodeberg NT, Sandberg SG, Johnson JA, Phillips PE, Wightman RM (2017) Hitchhiker's Guide to Voltammetry: Acute and Chronic Electrodes for in Vivo Fast-Scan Cyclic Voltammetry. *ACS chemical neuroscience* **8:** 221-234

Romano N, Guillou A, Hodson DJ, Martin AO, Mollard P (2017) Multiple-scale neuroendocrine signals connect brain and pituitary hormone rhythms. *Proceedings of the National Academy of Sciences of the United States of America* **114:** 2379-2382

Romano N, Yip SH, Hodson DJ, Guillou A, Parnaudeau S, Kirk S, Tronche F, Bonnefont X, Le Tissier P, Bunn SJ, Grattan DR, Mollard P, Martin AO (2013) Plasticity of hypothalamic dopamine neurons during lactation results in dissociation of electrical activity and release. *The Journal of neuroscience : the official journal of the Society for Neuroscience* **33:** 4424-4433

Stagkourakis S, Kim H, Lyons DJ, Broberger C (2016) Dopamine Autoreceptor Regulation of a Hypothalamic Dopaminergic Network. *Cell reports* **15:** 735-747

Stagkourakis S, Perez CT, Hellysaz A, Ammari R, Broberger C (2018) Network oscillation rules imposed by species-specific electrical coupling. *eLife* **7**

Stefaneanu L, Kovacs K, Scheithauer BW, Kontogeorgos G, Riehle DL, Sebo TJ, Murray D, Vidal S, Tran A, Buchfelder M, Fahlbusch R (2000) Effect of dopamine agonists on lactotroph adenomas of the human pituitary. *Endocr Pathol* **11:** 341-352

Sulzer D, Cragg SJ, Rice ME (2016) Striatal dopamine neurotransmission: Regulation of release and uptake. *Basal Ganglia* **6:** 123-148

Taylor D, Ho BT (1978) Comparison of inhibition of monoamine uptake by cocaine, methylphenidate and amphetamine. *Research communications in chemical pathology and pharmacology* **21:** 67-75

van den Pol AN, Cassidy JR (1982) The hypothalamic arcuate nucleus of rat--a quantitative Golgi analysis. *The Journal of comparative neurology* **204:** 65-98

Volkow ND, Fowler JS, Gatley SJ, Dewey SL, Wang GJ, Logan J, Ding YS, Franceschi D, Gifford A, Morgan A, Pappas N, King P (1999a) Comparable changes in synaptic dopamine induced by methylphenidate and by cocaine in the baboon brain. *Synapse* **31:** 59-66

Volkow ND, Wang GJ, Fowler JS, Fischman M, Foltin R, Abumrad NN, Gatley SJ, Logan J, Wong C, Gifford A, Ding YS, Hitzemann R, Pappas N (1999b) Methylphenidate and cocaine have a similar in vivo potency to block dopamine transporters in the human brain. *Life sciences* **65:** PL7-12

Zhang LF, Doyon WM, Clark JJ, Phillips PEM, Dani JA (2009) Controls of Tonic and Phasic Dopamine Transmission in the Dorsal and Ventral Striatum. *Molecular pharmacology* **76:** 396-404

Zhang XB, van den Pol AN (2015) Dopamine/Tyrosine Hydroxylase Neurons of the Hypothalamic Arcuate Nucleus Release GABA, Communicate with Dopaminergic and Other Arcuate Neurons, and Respond to Dynorphin, Met-Enkephalin, and Oxytocin. *Journal of Neuroscience* **35:** 14966-14982

Figures

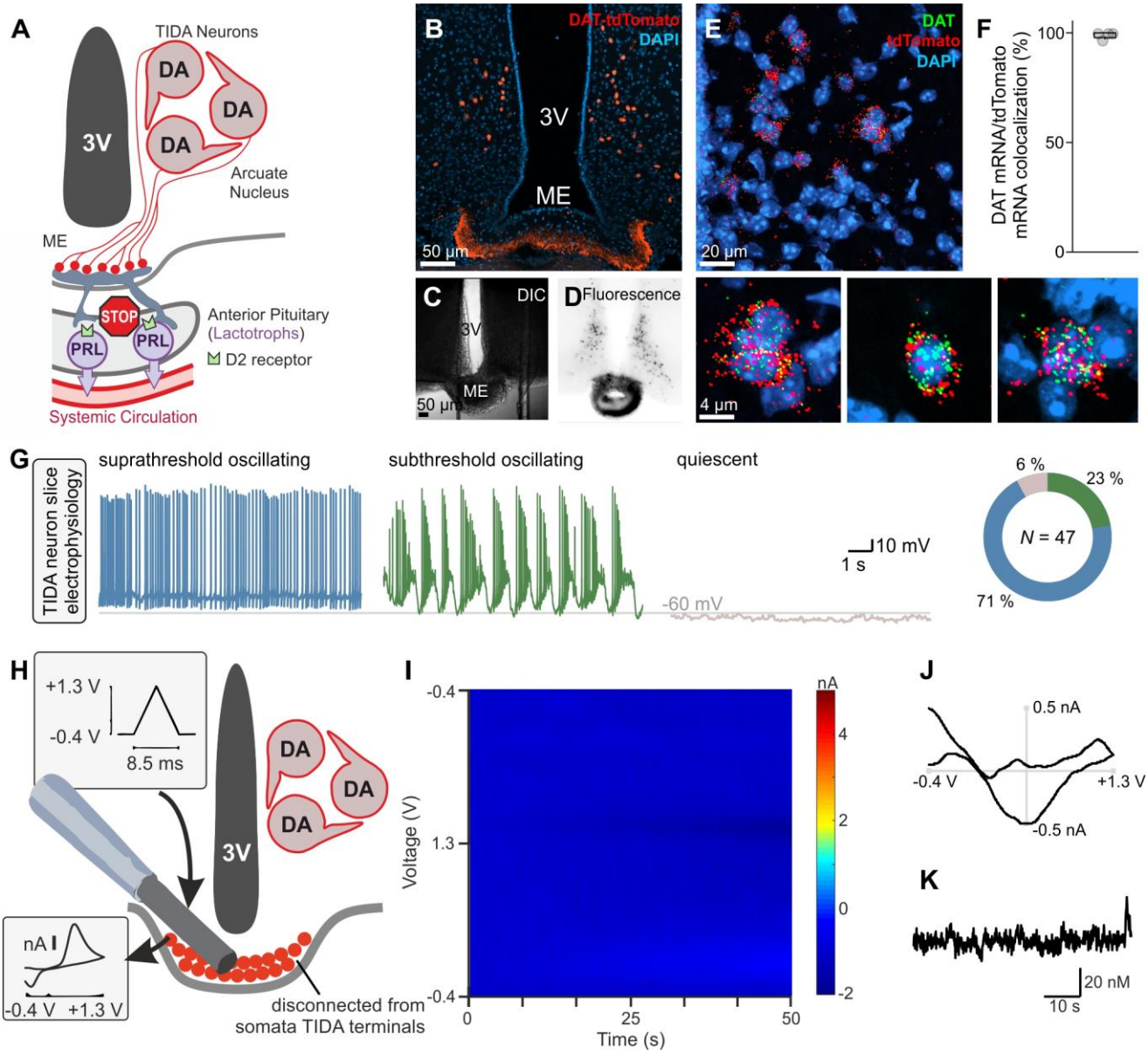

686

687 **Figure 1. TIDA neuron preparation and absence of detectable spontaneous dopamine**
688 **release in the median eminence (ME) in acute hypothalamic slices.** ***A,*** Schematic
689 illustration of the lactotrophic axis and the TIDA neuron projection to the median
690 eminence. ***B-D,*** Dopamine transporter (DAT) promoter-driven expression of tdTomato
691 for the identification of TIDA cells post-fixation (***B***) and in acute brain slices used for
692 electrophysiology visualized in differential interference contrast (DIC) (***C***), and in
693 fluorescence (***D***, converted to black and white and inverted) illumination, respectively.
694 ***E,*** *In situ* hybridization for the DAT and tdTomato mRNA to verify Cre-mediated
695 expression of floxed constructs in the DAT-Cre mouse line. ***F,*** Quantification of DAT and

tdTomato mRNA coexistence in cell bodies reveals a near 100% colocalization between the two transcripts (*N*=4 sections from 4 mice). ***G,*** Mouse TIDA neurons exhibit various patterns of activity, suprathreshold oscillations (left), subthreshold oscillations (middle) and quiescent behavior (right). Quantification of the proportion of TIDA neurons exhibiting the different forms of activity presented in the far right. ***H,*** Schematic drawing illustrating the use of fast-scan cyclic voltammetry and disc carbon electrodes to measure TIDA neural activity with neurotransmitter (dopamine) release in the ME. ***I-K,*** Representative color plot (*I*), voltammogram (*J*) and current *vs* time plot (*K*) generated through voltammetric measurements revealing no spontaneous dopamine release above detection threshold (5-10 nM) in the ME (*N*=20 recordings from *N*=10 slices from *N*=5 mice). 3V, third ventricle.

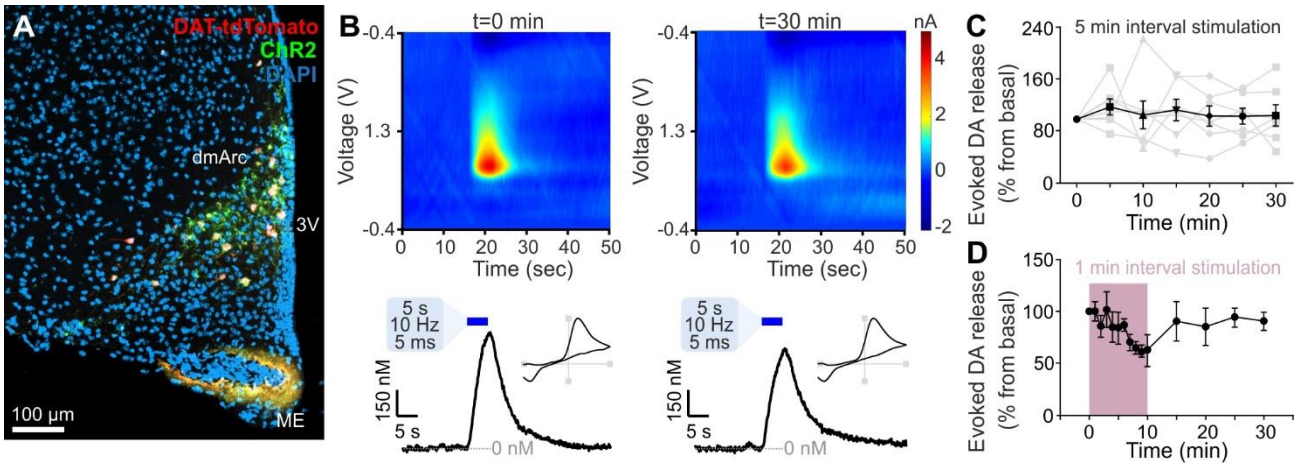

708

709 **Figure 2. Optogenetically evoked dopamine release in the median eminence is stable**
710 **over time.** ***A,*** Confocal Z-stack micrograph illustrating virally mediated ChR2-eYFP
711 expression in the dorsomedial arcuate nucleus (dmArc) in the DAT-tdTomato mouse.
712 Note the ChR2-eYFP and DAT-tdTomato fluorescence in the median eminence (ME). ***B,***
713 Optogenetically evoked dopamine release at t=0 min and 30 min after. ***C,*** Evoked
714 dopamine release with a 5-min stimulation interval is sustainable over time (*N*=7 per
715 group, RM one-way ANOVA, $p < 0.0001$; see also Table 1). ***D,*** Evoked dopamine release
716 with a 1-min stimulation interval leads to a reversible dopamine depletion, reversible
717 upon return to a 5-min stimulation interval (*N*=5 per group, RM one-way ANOVA, $p <$
718 0.0001). Data expressed as mean ± s.e.m. 3V, third ventricle.

719

720

721

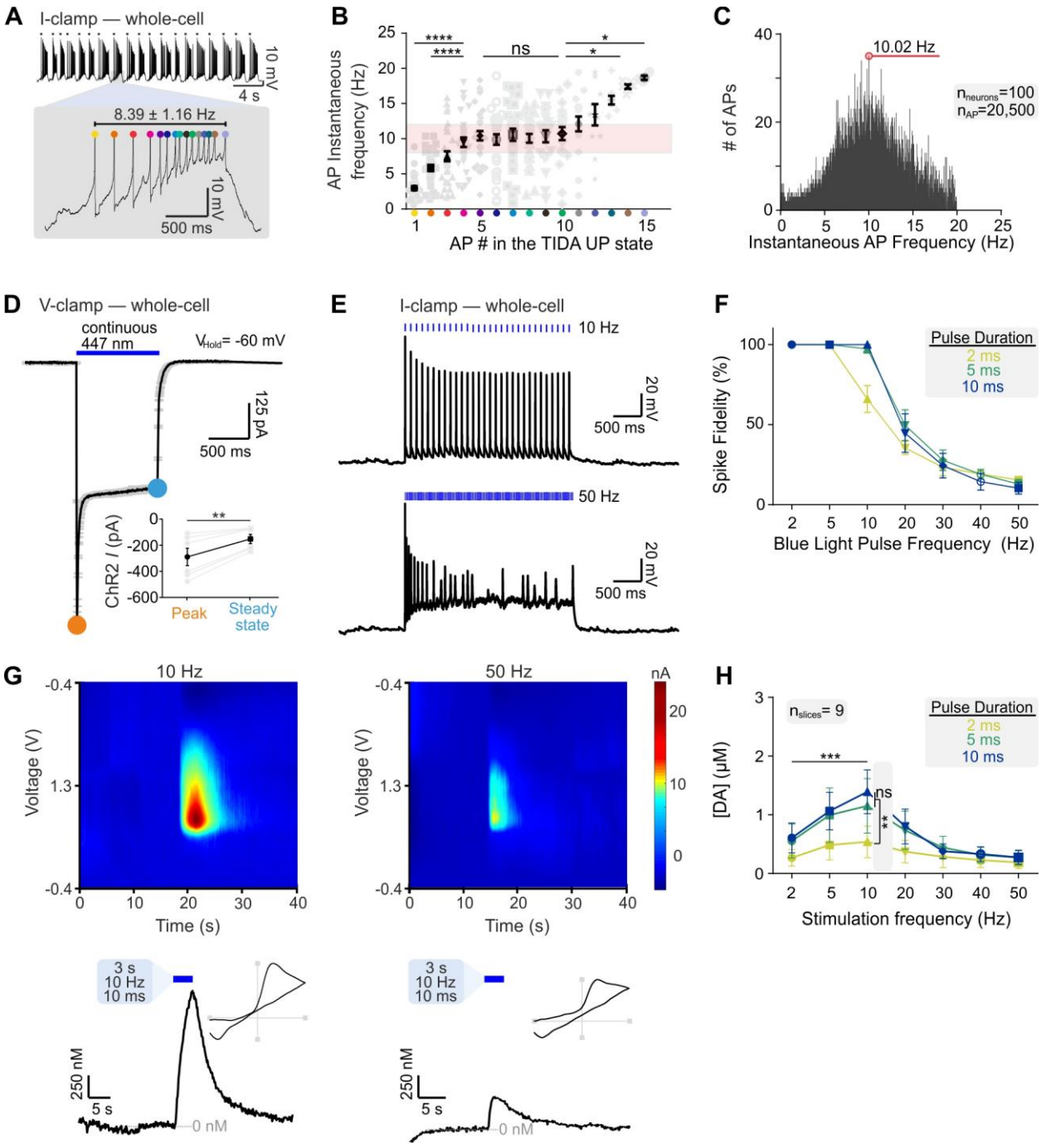

722

723 **Figure 3.** TIDA neuron endogenous firing frequency and optimal dopamine release in the
724 median eminence terminals occurs at 10 Hz. ***A,*** Whole-cell recording from a DAT-
725 tdTomato neuron, with one UP state shown in expanded temporal resolution (grey box
726 below; action potentials truncated for clarity). ***B,*** Quantification of the instantaneous
727 firing frequency (IFF) of action potentials (AP) in an UP state (*N*=33 cells, one-way

ANOVA, $p < 0.0001$; see also Table 1). ***C,*** Frequency distribution of IFF shows that the majority of spikes are discharged at 10 Hz. ***D,*** ChR2 current at the peak and steady state, mediated via 1s photostimulation (N=6, two-tailed paired t-test, $p = 0.0073$; see also Table 1). ***E,*** Representative traces with ChR2-driven AP firing at 10 Hz and 50 Hz. Note the depolarization block and low fidelity at 50 Hz. ***F,*** Quantification of spike fidelity *vs* photostimulation frequency and pulse width (RM one-way ANOVA, $p < 0.0001$; see also Table 1). ***G,*** Representative fast-scan cyclic voltammetry traces with ChR2-evoked dopamine release in the median eminence at 10 Hz and 50 Hz. ***H,*** Quantification of dopamine release in the median eminence *vs* photostimulation frequency and pulse width (RM one-way ANOVA, $p < 0.0001$; see also Table 1). *$p < 0.05$, **$p < 0.01$, ***$p < 0.001$, ****$p < 0.0001$. Data expressed as mean ± s.e.m.

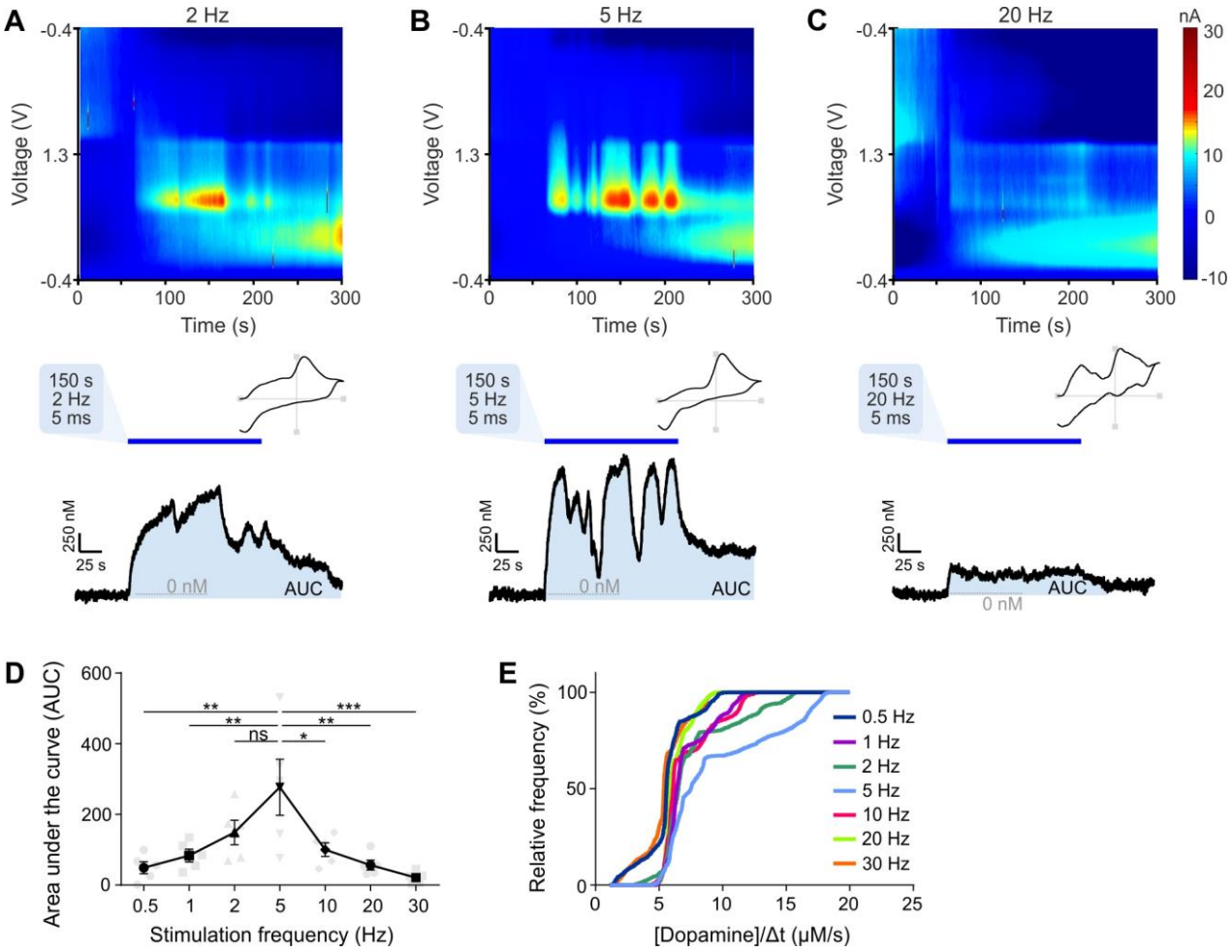

739

740 **Figure 4. In tonic firing configuration, TIDA terminals release maximal amounts of**
741 **dopamine in the median eminence at 5 Hz.** ***A-C,*** Representative fast-scan cyclic
742 voltammetry traces and heat maps with ChR2-evoked dopamine release in the median
743 eminence at 2 Hz, 5 Hz and 20 Hz. ***D,*** Quantification of dopamine release in the median
744 eminence *vs* photostimulation frequency with 5 ms pulse width (*N*=5, RM one-way
745 ANOVA, $p = 0.0004$; see also Table 1). ***E,*** Relative frequency of dopamine release per
746 second in the median eminence *vs* photostimulation frequency with 5 ms pulse width.
747 *$p < 0.05$, **$p < 0.01$, ***$p < 0.001$, ****$p < 0.0001$. Data expressed as mean ± s.e.m.

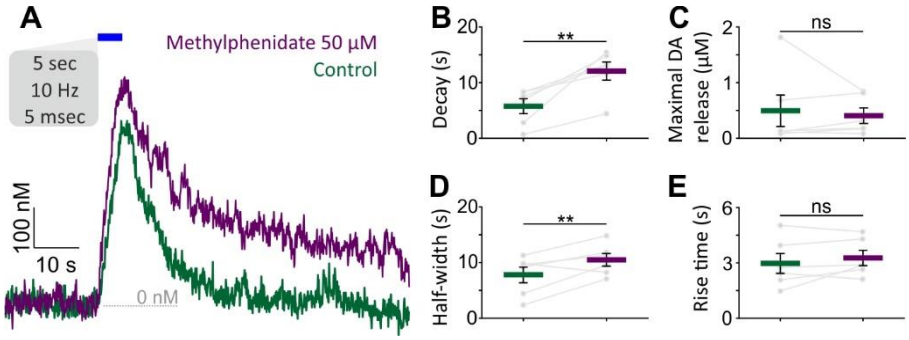

Figure 5. Dopamine release dynamics in the median eminence change upon dopamine transporter blockade. ***A,*** Representative dopamine-evoked oxidative current on baseline (green) and during (purple) dopamine transporter blockade with methylphenidate. ***B-E,*** Quantification of dopamine reuptake parameters such as decay (***B***), maximal amplitude of dopamine release (***C***), half-width (***D***), and rise time (***E***) (*N*=6, two-tailed paired *t*-test; see also Table 1). *$p < 0.05$, **$p < 0.01$, ***$p < 0.001$, ****$p < 0.0001$. Data expressed as mean ± s.e.m.

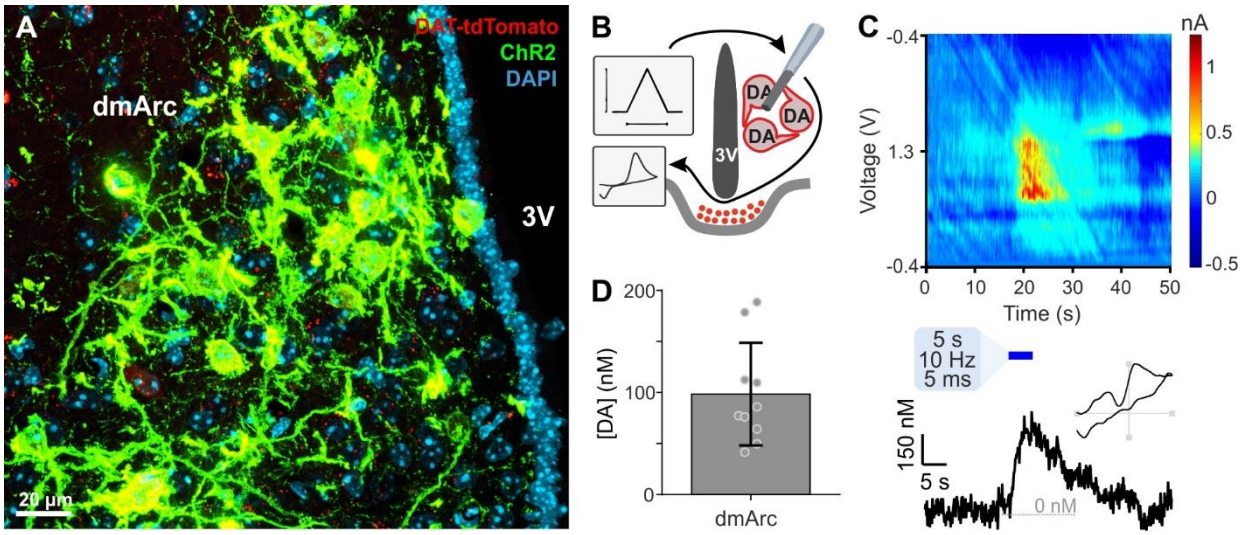

Figure 6. TIDA neurons release dopamine in the dorsomedial arcuate nucleus. ***A,*** Confocal Z-stack micrograph with virally mediated expression of ChR2-eYFP on DAT-tdTomato neurons in the dorsomedial arcuate nucleus (dmArc). ***B,*** Experimental design of fast-scan cyclic voltammetry recordings aiming to record evoked dopamine release in dmArc. ***C,*** Representative fast-scan cyclic voltammetry trace with ChR2-evoked dopamine release in the dmArc. ***D,*** Quantification of evoked-dopamine release in dmArc. Data expressed as mean ± s.e.m. 3V, third ventricle.

Table 1

Figures	Test	*N*	F or t values	Deg. of freedom	*p* value	Multiple comparisons	Adjusted *p* value	*p* value summary
Figure 2C	RM one-way ANOVA with Dunnett's multiple comparisons test	7	$F_{(3.161, 18.96)} = 0.2747$	6	0.8522	0 min vs. 5 min	0.5051	ns
						0 min vs. 10 min	0.9983	ns
						0 min vs. 15 min	0.8838	ns
						0 min vs. 20 min	0.9983	ns
						0 min vs. 25 min	0.9960	ns
						0 min vs. 30 min	0.9968	ns
Figure 2D	RM one-way ANOVA with Dunnett's multiple comparisons test	5	$F_{(3.036, 12.14)} = 2.188$	14	0.1413	0 min vs. 1 min	> 0.9999	ns
						0 min vs. 2 min	0.7617	ns
						0 min vs. 3 min	0.9999	ns
						0 min vs. 4 min	0.9156	ns
						0 min vs. 5 min	0.9098	ns
						0 min vs. 6 min	0.3838	ns
						0 min vs. 7 min	0.0835	ns
						0 min vs. 8 min	0.0256	*
						0 min vs. 9 min	0.0218	*
						0 min vs. 10 min	0.2914	ns
						0 min vs. 15 min	0.9977	ns
						0 min vs. 20 min	0.9725	ns
						0 min vs. 25 min	0.9941	ns
						0 min vs. 30 min	0.8931	ns
Figure 3B	Ordinary one-way ANOVA with Tukey's multiple comparisons test	33	$F_{(14, 338)} = 17.08$	14	< 0.0001	1 st vs. 4 th AP	< 0.0001	****
						2 nd vs. 4 th AP	< 0.0001	****
						5 th vs. 10 th AP	> 0.9999	ns
						10 th vs. 14 th AP	< 0.0132	*
						10 th vs. 15 th AP	< 0.0117	*

779

Figures	Test	Number of pairs	t value	Deg. of freedom	*p* value	*p* value summary
Figure 3D	Two-tailed paired *t* test	6	4.357	5	0.0073	**

Figures	Test	*N*	F or t values	Deg. of freedom	*p* value	Multiple comparisons	Adjusted *p* value	*p* value summary
Figure 3F (2 msec pulse duration)	RM one-way ANOVA with Dunnett's multiple comparisons test	6	$F_{(1.935, 9.677)} = 100.6$	6	< 0.0001	2 Hz vs. 5 Hz	> 0.9999	ns
						2 Hz vs. 10 Hz	0.0364	*
						2 Hz vs. 20 Hz	< 0.0001	****
						2 Hz vs. 30 Hz	0.0001	***
						2 Hz vs. 40 Hz	< 0.0001	****
						2 Hz vs. 50 Hz	< 0.0001	****
Figure 3F (5 msec pulse duration)		5	$F_{(6, 24)} = 100.4$	6	< 0.0001	2 Hz vs. 5 Hz	> 0.9999	ns
						2 Hz vs. 10 Hz	0.9932	ns
						2 Hz vs. 20 Hz	< 0.0001	****
						2 Hz vs. 30 Hz	< 0.0001	****
						2 Hz vs. 40 Hz	< 0.0001	****
						2 Hz vs. 50 Hz	< 0.0001	****
Figure 3F (10 msec pulse duration)		4	$F_{(1.503, 4.508)} = 72.97$	6	0.0004	2 Hz vs. 5 Hz	> 0.9999	ns
						2 Hz vs. 10 Hz	> 0.9999	ns
						2 Hz vs. 20 Hz	0.0595	ns
						2 Hz vs. 30 Hz	0.007	**
						2 Hz vs. 40 Hz	0.0016	**
						2 Hz vs. 50 Hz	0.0005	***

Figures	Test	*N*	F or t values	Deg. of freedom	*p* value	Multiple comparisons	Adjusted *p* value	*p* value summary
Figure 3H (2 msec pulse duration)	RM one-way ANOVA with Dunnett's multiple comparisons test	9	$F_{(1.111, 8.889)} = 4.124$	6	0.0706	2 Hz vs. 5 Hz	0.268	ns
						2 Hz vs. 10 Hz	0.3002	ns
						2 Hz vs. 20 Hz	0.2444	ns
						2 Hz vs. 30 Hz	0.2637	ns
						2 Hz vs. 40 Hz	0.7629	ns
						2 Hz vs. 50 Hz	0.4558	ns
Figure 3H (5 msec pulse duration)			$F_{(1.067, 8.536)} = 5.221$	6	0.0481	2 Hz vs. 5 Hz	0.1586	ns
						2 Hz vs. 10 Hz	0.0442	*
						2 Hz vs. 20 Hz	0.0852	ns
						2 Hz vs. 30 Hz	0.8233	ns
						2 Hz vs. 40 Hz	0.5971	ns
						2 Hz vs. 50 Hz	0.4555	ns
Figure 3H (10 msec pulse duration)			$F_{(6.00, 48.00)} = 11.77$	6	< 0.0001	2 Hz vs. 5 Hz	0.0509	ns
						2 Hz vs. 10 Hz	0.0002	***
						2 Hz vs. 20 Hz	0.7353	ns
						2 Hz vs. 30 Hz	0.6001	ns
						2 Hz vs. 40 Hz	0.416	ns
						2 Hz vs. 50 Hz	0.2369	ns

780

Figures	Test	*N*	F or t values	Deg. of freedom	*p* value	Multiple comparisons	Adjusted *p* value	*p* value summary
Figure 4D	Ordinary one-way ANOVA with Tukey's multiple comparisons test	5	$F_{(6, 28)} = 5.92$	6	0.0004	0.5 Hz vs. 1 Hz	0.9922	ns
						0.5 Hz vs. 2 Hz	0.4408	ns
						0.5 Hz vs. 5 Hz	0.0016	**
						0.5 Hz vs. 10 Hz	0.9448	ns
						0.5 Hz vs. 20 Hz	> 0.9999	ns
						0.5 Hz vs. 30 Hz	0.9973	ns
						1 Hz vs. 2 Hz	0.844	ns
						1 Hz vs. 5 Hz	0.0097	**
						1 Hz vs. 10 Hz	0.9999	ns
						1 Hz vs. 20 Hz	0.9979	ns
						1 Hz vs. 30 Hz	0.8659	ns
						2 Hz vs. 5 Hz	0.1787	ns
						2 Hz vs. 10 Hz	0.9559	ns
						2 Hz vs. 20 Hz	0.5291	ns
						2 Hz vs. 30 Hz	0.177	ns
						5 Hz vs. 10 Hz	0.0219	*
						5 Hz vs. 20 Hz	0.0024	**
						5 Hz vs. 30 Hz	0.0004	***
						10 Hz vs. 20 Hz	0.9734	ns
						10 Hz vs. 30 Hz	0.6909	ns
						20 Hz vs. 30 Hz	0.9907	ns

781

Figures	Test	Number of groups	Kruskal-Wallis statistic	*p* value	Multiple comparisons	Adjusted *p* value	*p* value summary
Figure 4E	One-way Kruskal-Wallis ANOVA	7	-22964	< 0.0001	0.5 Hz vs. 1 Hz	< 0.0001	****
					0.5 Hz vs. 2 Hz	< 0.0001	****
					0.5 Hz vs. 5 Hz	< 0.0001	****
					0.5 Hz vs. 10 Hz	< 0.0001	****
					0.5 Hz vs. 20 Hz	< 0.0001	****
					0.5 Hz vs. 30 Hz	< 0.0001	****
					1 Hz vs. 2 Hz	> 0.9999	ns
					1 Hz vs. 5 Hz	< 0.0001	****
					1 Hz vs. 10 Hz	< 0.0001	****
					1 Hz vs. 20 Hz	< 0.0001	****
					1 Hz vs. 30 Hz	< 0.0001	****
					2 Hz vs. 5 Hz	< 0.0001	****
					2 Hz vs. 10 Hz	< 0.0001	****
					2 Hz vs. 20 Hz	< 0.0001	****
					2 Hz vs. 30 Hz	< 0.0001	****
					5 Hz vs. 10 Hz	< 0.0001	****
					5 Hz vs. 20 Hz	< 0.0001	****
					5 Hz vs. 30 Hz	< 0.0001	****
					10 Hz vs. 20 Hz	< 0.0001	****
					10 Hz vs. 30 Hz	< 0.0001	****
					20 Hz vs. 30 Hz	< 0.0001	****

Figures	Test	Number of pairs	t value	Deg. of freedom	*p* value	*p* value summary
Figure 5B	Two-tailed paired *t* test	6	4.439	5	0.0068	**
Figure 5C	Two-tailed paired *t* test	6	0.4974	5	0.6400	ns
Figure 5D	Two-tailed paired *t* test	6	5.228	5	0.0034	**
Figure 5E	Two-tailed paired *t* test	6	1.115	5	0.3154	ns

784

785 *$p < 0.05$, **$p < 0.01$, ***$p < 0.001$, ****$p < 0.0001$